Passive Magnetic Localization in Medical Intervention

Zhenglong Sun, Luc Maréchal and Shaohui Foong

Abstract In the past decade, with continual advancement in the magnetic field sensing technology, passive magnetic tracking has become an emerging trend in the field of medical intervention. By embedding a small permanent magnet in the medical instrument, the passive magnetic tracking approach makes the system possible to have untethered, compact and wearable, even modular design for better ergonomics and lower hardware requirements. In this chapter, an overview of the working principle and methods of the passive magnetic tracking technology was presented. Implementation of the technology in actual medical interventions were also demonstrated. Lastly, the challenges in the development of this technology were explored and discussed.

1 Introduction

Motion tracking and navigation systems are paramount for both safety and efficacy in a variety of medical interventions and procedures. Magnetic field-based tracking technology becomes appealing for such applications. It utilizes the phenomenon that the distance and orientation of the magnetic source will change the amplitude and direction of the local magnetic field in space. By mapping the measurements of the local magnetic field to the distribution of the magnetic source, it is able to estimate up to six degrees-of-freedom (DOFs) positional information (both position

Z. Sun (✉)
School of Science and Engineering, The Chinese University of Hong Kong, Shenzhen,
2001 Longxiang Blvd, Longgang District, Shenzhen, China
e-mail: zhenglong.sun@ieee.org

L. Maréchal
SiMMS (Simulation and Modelling in Medicine and Surgery), Imperial College London,
369 Fulham Road, Chelsea and Westminster Hospital, London, UK
e-mail: l.marechal@imperial.ac.uk

S. Foong
Engineering Product Development, Singapore University of Technology and Design,
8 Somapah Road, Singapore, Singapore
e-mail: foongshaohui@sutd.edu.sg

H. Ren and J. Sun (eds.), *Electromagnetic Actuation and Sensing in Medical Robotics*,
Series in BioEngineering, https://doi.org/10.1007/978-981-10-6035-9_7

and orientation). Because the magnetic fields are of a low field strength and can safely pass through human tissue with least interference, it can be used for tracking instruments/tools inside the human body without line-of-sight restrictions.

In general, based on the type of the magnetic source, the tracking techniques can be divided into two groups: active electromagnetic (EM) tracking and passive magnetic tracking. In active electromagnetic tracking, the magnetic source is generated by excitation coils; while in passive magnetic tracking, the magnetic source is from a permanent magnet. Although both groups are often referred as *magnetic tracking*, the underlying principles are fundamentally different [4]. Several tracking systems based on the active approach have been commercially available. It requires sending a small sensor coil (e.g. AURORA system, NDI Medical, US) or an EM transmitter (e.g. CORTRAK system, Corpak Medsystems, US) together with the medical instrument into the human body. The source will generate controlled, varying electromagnetic field. Small voltage signals will be induced in the sensor coil, and therefore be characterized to calculate the position and orientation of the sensor. In this process, tethering wires are usually indispensable for power supply as well as electrical signal transmission. In comparison to that, the passive magnetic tracking provides a less-invasive option. It only requires associating a small permanent magnet with the medical instrument as the passive source, and all electronic components (such as the magnetic sensors) can be left outside the human body. By measuring the magnetic fields at fixed points in space, the position, and orientation of the permanent magnet can be calculated. In such manner, the system can be designed to be completely untethered and wireless. Because of this feature, passive magnetic tracking approach has been adopted in many medical research studies, such as the wireless capsule endoscope [14, 22], heart valve prostheses [1], ventriculostomy [11] and nasogastric intubation [2, 20].

Therefore, in this chapter, the magnetic field model often used in passive magnetic tracking is first reviewed. Then two different localization methods are described, namely the inverse optimization method and the direct ANN (artificial neural network) method; the advantages and disadvantages of the two methods are discussed using two actual medical intervention procedures for practical illustration. Lastly, some limitations and challenges faced by the passive magnetic tracking are discussed.

2 Modeling the Magnetic Field of Permanent Magnet

2.1 Dipole Model

Same as in the active EM tracking technique, the magnetic source is often modeled by a magnetic dipole as shown in Fig. 1. The Dipole Model (originally suggested by Fitz Gerlad in 1883) is commonly adopted in these works for its simplicity. Schlageter et al. first presented a 5-DOFs tracking system with 4×4 2D-array of Hall sensors [15]. Hu et al. evaluated different nonlinear optimization methods in

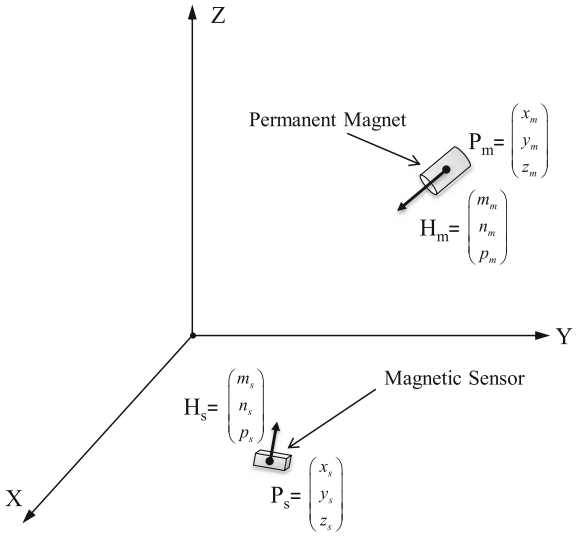

Fig. 1 Illustration of modeling the permanent magnet as a single magnetic dipole.

tracking 3D location and 2D orientation of the capsule endoscope movement [7]. Yao et al. demonstrated the detection of magnetic object with a fixed three-axial Hall probe for tracking control [26]. Lee et al. developed a magnetic gradient tensor method to detect ferromagnetic objects for guiding the visually impaired [8, 9]. Researches have also been done in the sensor arrangement and optimization to achieve higher tracking accuracy [6, 12, 13].

In Dipole Model, the total magnetic flux density at ith observation point (magnetic sensor) due to the magnetic dipole is modeled as

$$\mathbf{B}(\mathbf{P}_{s_i}) = \frac{\mu_r \mu_0 \cdot M}{4\pi} \left(\frac{3(\mathbf{H}_m \cdot \mathbf{P}_i)\mathbf{P}_i - R_i^3 \cdot \mathbf{H}_m}{R_i^5} \right), \tag{1}$$

where μ_r is the relative permeability of the medium, μ_0 is the magnetic permeability of free space (mT· mm/A), M is the constant strength of the dipole moment (A· mm^2) measured from the permanent magnet, $\mathbf{H}_m$ is a unit vector along the magnet magnetization axis. and $\mathbf{P}_i$ is a vector from the magnet $\mathbf{P}_m$ pointing to the ith sensor $\mathbf{P}_s^i$, and R_i is the magnitude of the vector $\mathbf{P}_i$,

$$\mathbf{P}_i = \mathbf{P}_{s_i} - \mathbf{P}_m. \tag{2}$$

Dipole model is known for its simplicity, since it has only one unknown parameter, the dipole moment strength M. Usually it is considered to be constant, and can be decided by the material magnetic field strength and the magnetic object volume.

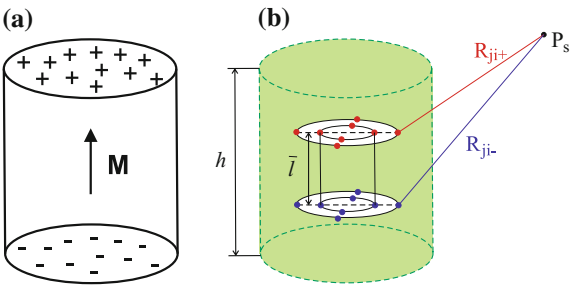

Fig. 2 Illustration of **a** the Charge Model and **b** the Distributed Multipole Model of a cylindrical permanent magnet.

2.2 Charge Model

While the dipole model has been widely adopted, it ignores the geometry of the permanent magnet and it gives poor approximation of the near field of the magnet. In general, it is often studied best for needle-like magnets, or the distance is sufficiently larger than the dimension of the magnet. To account for the geometry of a permanent magnet, the Charge Model can be used. In the Charge Model, the magnet is modeled as a distribution of equivalent "*magnetic charge*" as shown in Fig. 2a. It is derived from the magnetostatic field equations, and the fields are obtained using standard methods [5]. It defines two parameters

$$\begin{aligned} \rho_m &= -\nabla \cdot \mathbf{M} \ \ (A/m^2) \qquad \text{(volume charge density)} \\ \sigma_m &= \mathbf{M} \cdot \hat{\mathbf{n}} \ \ (A/m) \qquad \text{(surface charge density)}, \end{aligned} \tag{3}$$

where $\mathbf{M} = M_s \mathbf{H}_m$ is the magnetization, and $\hat{\mathbf{n}}$ is the outward unit normal vector. Considering a magnet is free space, the magnetic flux density at observation point $\mathbf{P}_s$ can be written as

$$\mathbf{B}(\mathbf{P}_s) = \frac{\mu_0}{4\pi} \int_V \frac{\rho_m(\mathbf{P}_c)(\mathbf{P}_s - \mathbf{P}_c)}{|\mathbf{P}_s - \mathbf{P}_c|^3} dv' + \frac{\mu_0}{4\pi} \oint_S \frac{\sigma_m(\mathbf{P}_c)(\mathbf{P}_s - \mathbf{P}_c)}{|\mathbf{P}_s - \mathbf{P}_c|^3} ds', \tag{4}$$

where $\mathbf{P}_c = [x_c, y_c, z_c]^T$ is the source point (the surface magnetic charge).

For a constant magnetization in a magnet, the volume charge density ρ_m equals to zero, and the magnetic field can be calculated by integration of the surface charge density. In such manner, both the shape and the magnetization of the magnet will contribute to the magnetic field calculation.

2.3 Distributed Multipole Model

Distributed Multipole (DMP) model is another method that is often used to account for the shape and magnetization of a permanent magnet. It was firstly proposed and

generalized in [10]. In the DMP model, a *dipole* is defined as a pair of source and sink separated by a distance $\bar{l}$. And it may contain multiple k loops (or columns) of n dipoles distributed within the magnet volume, as shown in Fig. 2b.

The magnetic flux density at any point $\mathbf{P}_s$ contributed by all the dipoles (in terms of the ith dipole in the jth loop) is thus given by

$$\mathbf{B}(\mathbf{P}_s) = \sum_{j=0}^{k} \sum_{i=0}^{n} M_{ji} \beta_{ji}, \tag{5}$$

Here M_{ji} is the strength of the jith dipole, and the term β_{ji} represents

$$\beta_{ji} = -\frac{\mu_0}{4\pi} \left(\frac{\mathbf{a}_{R_{ji+}}}{R_{ji+}^2} - \frac{\mathbf{a}_{R_{ji-}}}{R_{ji-}^2} \right), \tag{6}$$

where $\mathbf{a}_R = \mathbf{R}/R$, and R_{ji+} and R_{ji-} expressed in terms of distance $\bar{l}$ are the distances from the source and sink of the jith dipole to the observation point $\mathbf{P}_s$.

The unknown parameters in (5) are the number of dipoles per loop n, the loop number k, the separation distance between the source and sink $\bar{l}$, and the strength of the moment for each dipole m_{ji}. Given more degrees of freedoms, the DMP model outperforms the Dipole Model in depicting the magnetic field of a permanent magnet of random shape and magnetization; but all the parameters have to be calculated accordingly through proper calibrations, since there is no physical meaning behind the distributed dipoles.

2.4 Hybrid Model

Although the model accuracy deteriorates as it approaches the surface of the magnet, the Dipole Model is still able to adequately characterize the magnetic field at large distances from the source for many applications. Therefore, a hybrid model has been proposed by Wu et al. to keep the simplicity of the model while compensating for the incompetence of the Dipole Model at near field [23].

In this hybrid model, non-parametric Artificial Neural Network (ANN) model is employed to depict the magnetic field in spatial areas at close proximity to the magnet; and the parametric Dipole model is employed at spatial locations sufficiently far away from the magnetic source. By exploiting the magnetic field of an axisymmetric permanent magnet in cylindrical coordinates as elaborated in Fig. 3, the workload for data collection and training for the ANN model can be reduced significantly. In order to ensure smooth transition between the two models in the hybrid model, the magnetic equipotential (region in free space where every point is at the same potential, i.e., B = constant) is used. The concept of the hybrid model is as shown in Fig. 4.

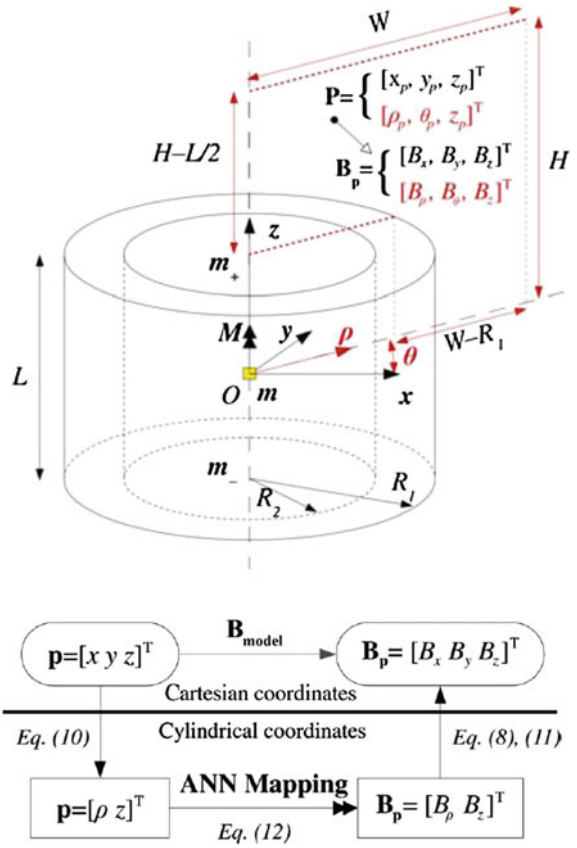

Fig. 3 Schematic illustration of the magnetic field of an axisymmetric cylinder/annular magnet (above) and the ANN mapping process with conversions between Cartesian and Cylindrical Coordinates (below). W and H representing the width and height of the field, while L and R representing the length and radius of the magnet respectively.

Here a potential threshold B_{th} is introduced. By observing the magnetic field B_p as measured at location $\mathbf{p}$, the ANN model will be used if $B_p \geq B_{th}$ (closer to the magnet) and Dipole model will be used if $B_p \leq B_{th}$ (further away from the magnet). A sigmoid function is used together to determine the percentage of contribution from the two models as shown below,

$$B_{hybrid} = B_{ANN} \times y + B_{Dipole} \times (100 - y), \tag{7}$$

where the percentage y is expressed as

$$y = 50\left[\frac{B_p - B_{th}}{\sqrt{A + (B_p - B_{th})^2}} + 1\right]. \tag{8}$$

In such manner, the hybrid model is able to maintain the modeling accuracy at locations near the magnet, and retain the capability of extrapolating the fields using

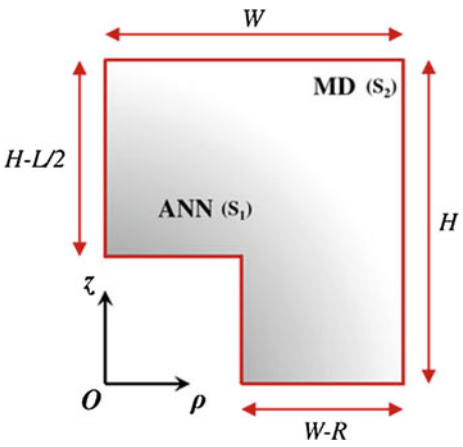

Fig. 4 Illustration of the hybrid model of a cylindrical magnet in the transverse plane. ANN model region (S_1) and Magnetic Dipole (MD) model region (S_2) segregate along the equipotential line.

the simple parametric Dipole model. The hybrid model is also able to account for the geometry and size of the permanent magnet, but the method discussed here is only optimized for axisymmetric magnetic object. It is worthy to note that it can be easily generalized to arbitrary geometry and magnetization if needed. Still pre-calibration procedure is required for the ANN model, and re-calibration of the Dipole model might be necessary for best performance.

3 Principle of the Passive Magnetic Tracking

Previous section demonstrated some of the mathematical models that are often adopted to depict the magnetic field of a permanent magnet. The inputs to these models are the positional information (both position and orientation) of the magnetic source (e.g. the permanent magnet) and the observation point (e.g. the sensor) in space, while the outputs are the magnetic field at the observation point (e.g. the sensor measurement). However, due to the non-linearity of the models, there is no analytical solution to the inverse function to retrieve the positional information directly from the sensor measurement. In the following, two distinct tracking principles are reviewed and discussed.

3.1 Inverse Optimization Method

Inverse optimization method requires solving an inverse problem as illustrated in Fig. 5. The sensors measurements are used to compare with the estimation results by feeding positional information into the magnetic field models. A cost function C

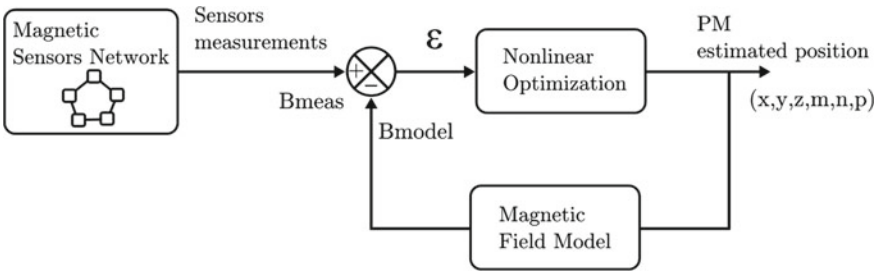

Fig. 5 Principle of passive magnetic localization with inverse optimization method.

is then defined to quantify the differences between the measured and the modeled magnetic field at all k sensors in the sensor array:

$$C = \sum_{i=1}^{k} ||\mathbf{B}_{modeled}(\mathbf{P}_{s_i}) - \mathbf{B}_{measured}(\mathbf{P}_{s_i})||^2. \tag{9}$$

Then the positional information of the magnetic source can be calculated through nonlinear optimization in a least-square manner. By minimizing this cost function through iterative optimization, the position vector $\mathbf{P}_m$ and orientation $\mathbf{H}$ of the permanent magnet can be estimated.

As illustrated in Fig. 1, $\mathbf{H}$ represents a unit vector along the magnetized axis of the permanent magnet, so the three components of $\mathbf{H}$ are actually correlated:

$$m^2 + n^2 + p^2 = 1. \tag{10}$$

Therefore, at least five sensor measurements are required in order to solve the position and orientation information of the permanent magnet. Often more sensors are used to increase the system redundancy for better resilience against environment and hardware noises. It is noted that only five DOF information can be retrieved as elements in the orientation vector $[m, n, p]$ are coupled. This is because the magnetic field models are in particular axis-symmetric about the magnetization axis of the permanent magnet.

The inverse optimization method is widely adopted in a number of research and applications. It is easily to be implemented, with no or little pre-procedural preparation is required, and no specified workspace is needed. The accuracy of the tracking depends on the adequacy of the magnetic field model used, the convergence of the optimization algorithm adopted, and the robustness of the magnetic sensors employed. In general, complexity of the field model and computational expensiveness of the optimization algorithm may lead to a compromise between the requirements of tracking accuracy and processing speed.

3.2 Direct ANN Method

Contrary to a physical model, the ANN model is a non-parametric model that is inspired by biological neural networks. It consists of artificial neuron as a fundamental information processing unit in the neural network structure. At each neuron, it contains one or more input signals $(x_1, x_2, \cdots, x_n)$ associating with weights $(w_1, w_2, \cdots, w_n)$ and one output signal y. Mathematical representation of this model at kth neuron can be written as

$$y_k = g(\sum_{j=1}^{n} w_{ki} x_i), \tag{11}$$

where function g is a nonlinear activation function, such as a sigmoid function [3].

The output of each neuron is computed and propagated through all the hidden layers. In practice, the implementation of direct ANN method accepts n magnetic sensors field data as inputs $(B_{x1}, B_{y1}, B_{z1}, ..., B_{xn}, B_{yn}, B_{zn})$ and directly produces the position and orientation of the permanent magnet (x, y, z, m, n, p) as outputs as illustrated in Fig. 6. Basically, the ANN consists of sets of adaptive weights, which requires supervised learning from pre-procedural training. Once the training is done, the outputs can be directly obtained by performing linear transformation of the inputs. Compared to the traditional inverse optimization method, the direct ANN method bypasses the solving of the challenging inverse problem. Moreover, it can directly incorporate the intrinsic characteristics of the sensors, such as the sensor precision and noise. In such a manner, the direct ANN method is able to provide straightforward and fast calculation with high accuracy. But on the other hand, the direct ANN method also poses the requirement of pre-procedural data collection and training within the region-of-interest (ROI). Therefore, for each medical intervention, determining an *ad hoc* ROI for training is crucial for the direct ANN method in order to reduce the workload for the pre-procedural data collection and training process. In a nut shell,

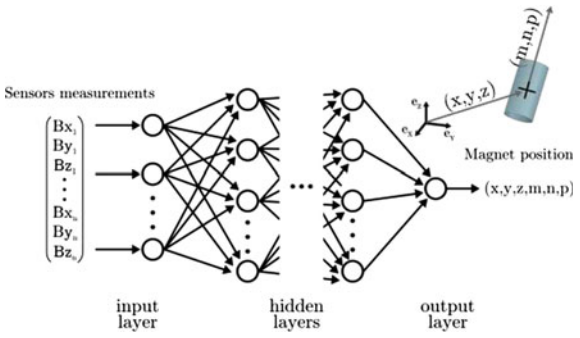

Fig. 6 Principle of passive magnetic localization with direct ANN method.

the direct ANN method provides an ideal solution for those medical interventions with relatively low variance in trajectory but requirements of high accuracy and real-time tracking.

4 Implementation of the Passive Magnetic Tracking in Medical Applications

In this section, two medical intervention procedures are presented to illustrate the implementation of the passive magnetic tracking in practical medical applications:

- The Ventriculostomy, also known as External Ventricular Drain (EVD), which requires inserting a catheter through a burr hole on the skull into the brain tissue to access brain ventricles.
- The Nasogastric (NG) intubation, which consists of inserting a flexible hollow tube through the nose, past the throat and down into the stomach.

Illustrations of two medical intervention procedures are shown in Fig. 7. The problem in the conventional routines for both procedures is that they are manually performed "blind" by clinicians without any visual aids or indications. Without real-time instrument tracking, it may result in safety risks in identifying erroneous insertions, which could potentially cause significant complications and even morbidity. By embedding a small permanent magnet at the tip of the catheter, the passive magnetic tracking could be applied to provide real-time monitoring of the position and orientation information of the magnet at the tip of the catheter. In such manner, the system would allow untethered instrument tracking. It is expected that potential erroneous insertions could be prevented and corrected right away; thus, the success rate of the intervention procedures could be improved.

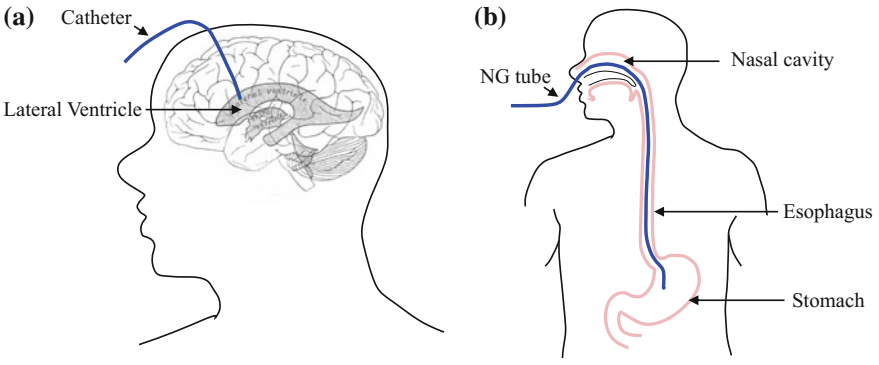

Fig. 7 **a** The Ventriculostomy **b** the Nasogastric (NG) intubation.

In the following, implementation of the passive magnetic tracking in these two procedures are presented. Experiments were carried out on specifically designed localization systems. Both the traditional inverse optimization method and the direct ANN method were applied in tracking random conical-helix paths and representative medical specific trajectories. Tracking performance of the two distinct methods was then assessed and compared.

4.1 Localization Systems and Experimental Setup

For each application, a customized localization system with embedded sensor array was designed and built. As shown in Fig. 8, for the Ventriculostomy procedure, eight sensors were used and arranged in a specific pattern on a flat circular board around the burr hole on the skull for the catheter to go through; for the NG intubation, eleven sensors were used and distributed inline on a semi-circular neck attachment (radius 65 mm with sensor spacing 15°), where the center sensor laid on the thyroid cartilage with its surface perpendicular to the neck.

To experimentally test the localization performance, a bench test was set up, as featured in Fig. 9. A Grade N52 Neodymium (Nd-Fe-B) magnet from K&J Magnetics (Jamison, PA, USA) was mounted at the end-effector of a 6-axis articulated robotic arm (VS-068, Denso Robotics, Aichi, Japan). The dimensions of the permanent magnet (3.2 mm diameter and 9.5 mm length) were chosen to fit the inner diameter of the catheter. An off-the-shelf digital 3-axis magnetic sensor, MAG3110 (Freescale Semiconductor, Austin, USA) was employed for its high sensitivity to low magnetic field measurement, with a resolution of 0.10 μT and a range of ± 1000 μT. The sensors measurements were then acquired by a real-time controller cRIO 9082 (National Instruments, Austin, USA). With a positional repeatability of ± 0.02 mm, the robotic arm was commanded to accurately move the magnet along reference trajectories in designed configuration (both position and orientation).

Same sets of experimental data were concurrently tested on the two methods: the inverse optimization method and the direct ANN method. For the direct ANN method, a ROI for pre-procedural data collection and training was firstly decided based on the specifications of corresponding medical application. For example, for Ventriculostomy procedure the catheter is inserted through a small hole in the skull. Consequently, the whole expected tracking ROI for Ventriculostomy can be reasonably defined as a cone. The possible orientations of the magnet can also be limited regarding the physical constrains of the catheter, which is unlikely to bend an angle exceeding 45° from the axial plane. The same approach can be applied for NG intubation where the ROI can be represented by a tube encompassing the esophagus and trachea. Hence, the orientation of the magnet is highly limited around the sagittal axis. The spatial resolution within the ROI was set at 1 mm. At each position, instead of testing different configurations, a random orientation $[m, n, p]$ of the magnet about its magnetization axis was assigned within a designed range, in order to include as much as variations without significantly increasing the number of training data sets.

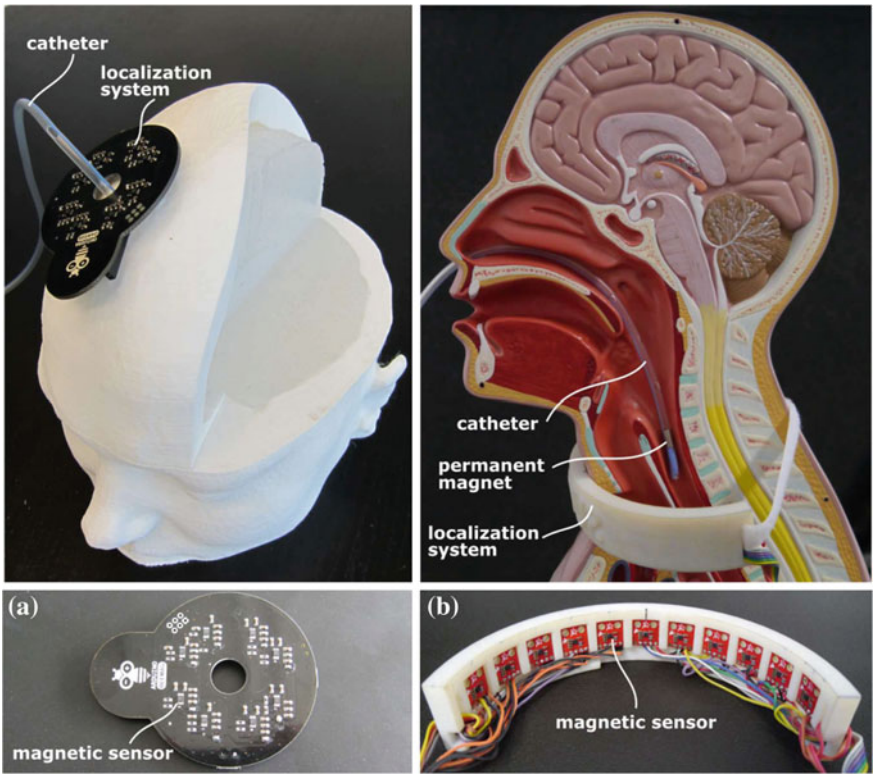

Fig. 8 Design and installation of the localization systems for two different medical interventions **a** Ventriculostomy **b** the Nasogastric (NG) intubation.

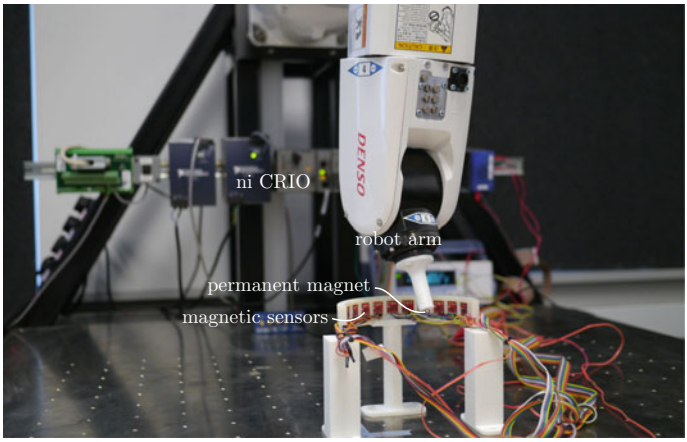

Fig. 9 Experimental setup for tracking performance tests. The six-axis robotic arm provides the ground truth localization of the permanent magnet.

Table 1 ROI parameters for two medical applications.

Parameters	Ventriculostomy	NG Intubation
Volume (cm^3)	90	60
Number of points	52811	19530
Range m	[0, 0.4]	[−0.1, 0.3]
Range n	[−0.2, 0.2]	[−0.1, 0.1]
Range p	[−1, −0.6]	[−1, −0.8]
Calibration time (hour)	13	5

The detailed parameters of the ROI for both applications are shown in Table 1. Neural network toolbox from MATLAB (Mathworks, USA) was used to train the data sets with ten hidden layers and Levenberg-Marquardt back propagation algorithm. For the inverse optimization method, the Dipole model was used for its simplicity and fast calculation processing speed; and Levenberg-Marquardt Algorithm was used as the optimization algorithm.

4.2 Experimental Results

The tracking performance of both methods can be visualized in Figs. 10 and 11, where the true reference trajectory in solid line, the estimated trajectory in colored dots. In Fig. 10, non-application specific conical-helix paths were tested for both procedures. For the Ventriculostomy procedure, the center of the circular sensor board was placed at (0, 0, 0); for the NG intubation procedure, the center of the semi-circular attachment was placed at (0, 0, 0) with the opening towards the positive X-axis direction. In Fig. 11, medical representative trajectories based on *in situ* data from either real patient or realistic manikin dummy were tested. In this case, the coordinates of the localization system were planned according to the actual settings. For the Ventriculostomy procedure, the sensor board was placed on the top right corner where the trajectory went through the center hole; for the NG intubation procedure, the center of the attachment remained at (0, 0, 0) but the attachment was placed perpendicular to the neck with 20° above the positive X-axis direction.

Table 2 summarizes the RMSE (root mean square error) and the maximum localization error along different paths tested. It can be seen that both methods are able to track the reference trajectories. It can be seen that the direct ANN method outperforms the traditional inverse optimization method in terms of localization accuracy in all cases. The RMSE of the tracking error using the direct ANN method can be as small as less than 2 mm. Higher errors were seen in the NG intubation system for both localization methods. That is because the Euclidean distance between the passive source (permanent magnet) and the sensors are generally farther in the NG intubation system, resulting in lower Signal-to-Noise Ratio (SNR). This can be seen

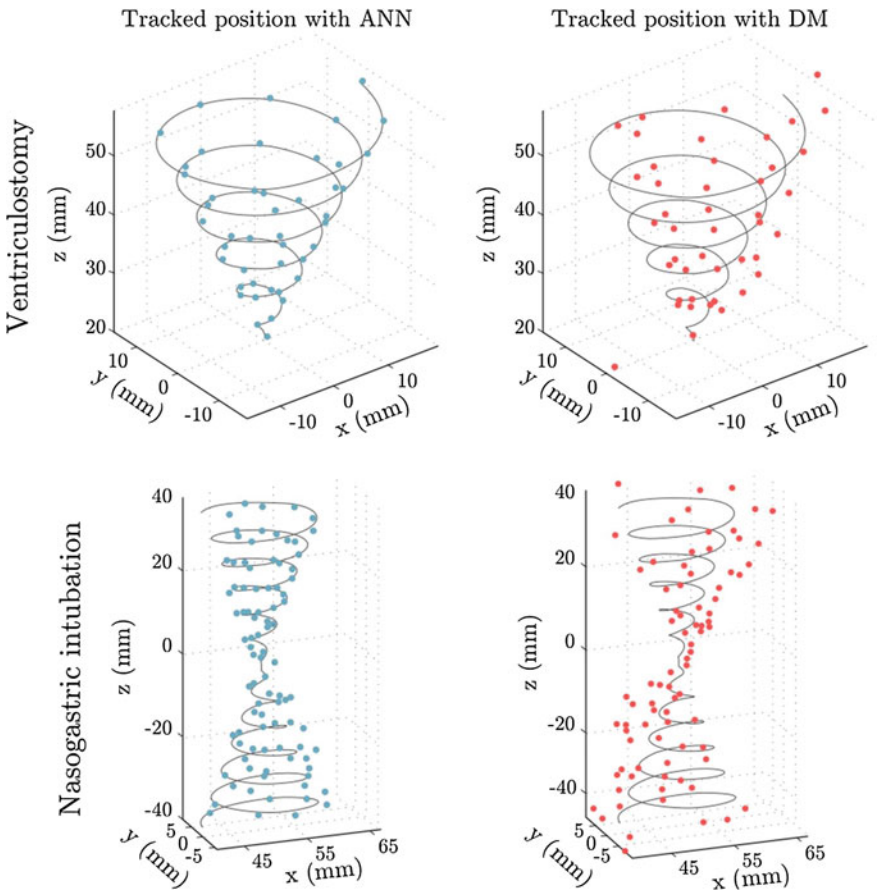

Fig. 10 Performance of the passive magnetic tracking of non-application specific conical-helix path in two different medical applications using the direct ANN method (left) and the inverse optimization method (right).

from Fig. 12, where the localization errors for all trajectories were plotted against the Z-axis (considering as the penetration direction). It is also shown that the SNR has much higher influences on the inverse optimization method than on the direct ANN method. Significantly increases in the localization error can be observed as the source moved away from the sensors when the inverse optimization method was used, but the localization error remained on the same level throughout the range for the direct ANN method. However, such robustness requires pre-procedural data collection and training within the defined ROI.

It is also noted that in Fig. 11, when the inverse optimization method was used in Ventriculostomy procedure, the first few points were off the reference trajectory. That is because some of the sensors readings were saturated as the magnet passing through the center hole and getting too close to the sensors. Such adverse sensor readings

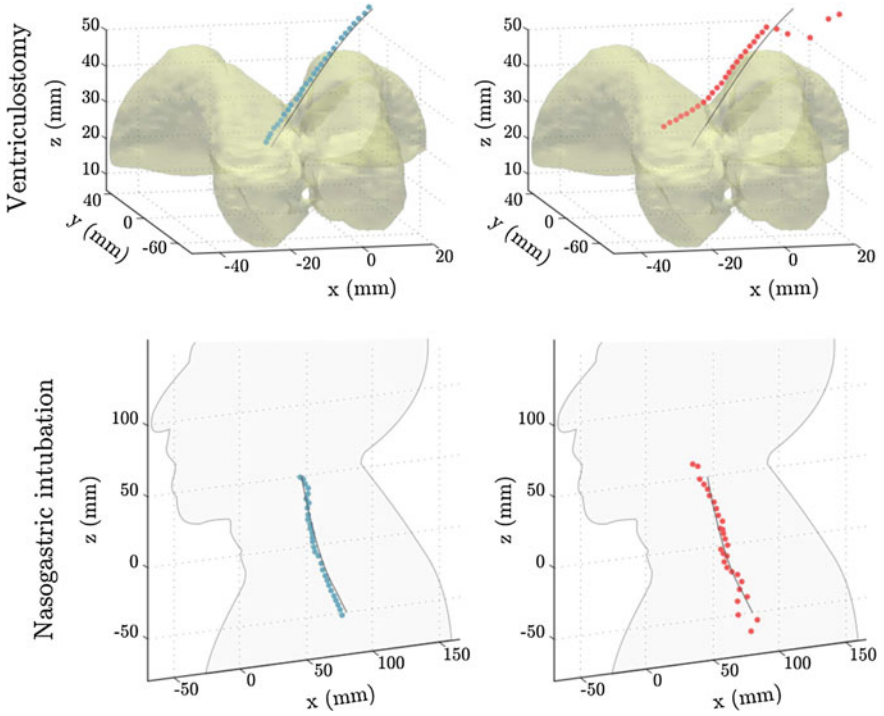

Fig. 11 Performance of the passive magnetic tracking of medical representative trajectories in two different medical applications using the direct ANN method (left) and the inverse optimization method (right).

Table 2 Tracking performance of two methods in different medical applications.

Tracking paths	Methods	Inverse optimization method		Direct ANN method	
	Procedures	Ventriculostomy	NG Intubation	Ventriculostomy	NG Intubation
Non-specific conical-helix	RMSE (mm)	9.8	6.4	0.8	1.5
	Max (mm)	14.3	17.2	1.2	5.3
Representative trajectory	RMSE (mm)	5.8	6.8	1.1	1.8
	Max (mm)	12.9	15.4	1.6	4.5

could affect the convergence in the optimization algorithm, resulting in erroneous estimation. Thus, it requires control algorithm for real-time sensor fault detection and correction [16, 21]. In comparison, as long as the trajectory was covered by the trained ROI, the direct ANN method was able to take account of the adverse sensor readings such as saturation.

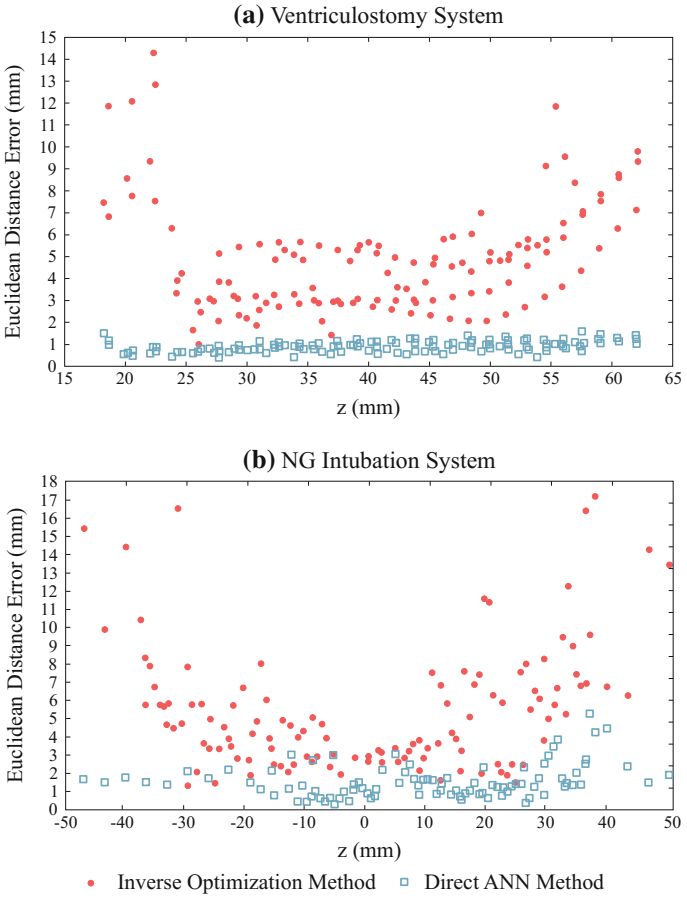

Fig. 12 Euclidean distance errors for conical-helix path and representative trajectory altogether along the insertion direction **a** Ventriculostomy System **b** NG Intubation System.

4.3 Discussions on the Method Selection

Implementation of the passive magnetic tracking has been demonstrated in two medical intervention examples. Both the inverse optimization method and the direct ANN method were used. In general, the direct ANN method provides higher tracking accuracy, at the cost of pre-procedural training. Thanks to its non-parametric nature, the direct ANN method is able to take account of the sensor characteristics; but also because of that, the direct ANN method can only be implemented within the ROI where the pre-procedural calibration was performed in. In order to have larger tracking region, more data points have to be measured for training, resulting in prolonged data collection process and increased training complexity. But once the preparation work is done, the computation of the ANN would be linear transformation from the

inputs to the outputs; implementation of the method would be straightforward and fast. In comparison, the inverse optimization method is based on a physical model of the permanent magnet. It only requires calibration of the model parameter(s), then it can be implemented at any point in space. However, the tracking accuracy would be greatly affected by the modeling errors. More sophisticated models can be used to increase the model accuracy, but the model complexity would greatly affect the processing speed as the inverse optimization algorithm requires iterative computations.

In a nutshell, both methods could be used in realization of untethered medical instrument tracking. The selection of the methods for the tracking is driven by the variation of the intervention trajectory, the size of the ROI, the requested tracking accuracy and the refresh rate. Generally speaking, the direct ANN method is more accurate and versatile, requiring application specific pre-procedural training but offering fast processing in real-time; the inverse optimization method is more adaptive but more computationally intensive. If the ROI is relatively small, the required accuracy is high and most importantly the measurement conditions are consistent, the direct ANN method is preferable. Though when the tracking area is large, the path has high variance or the accuracy is less critical, the inverse optimization method is better to be considered.

5 Challenges and Outlook of the Passive Magnetic Tracking

There are quite a number of advantages of adopting passive magnetic tracking technology in medical applications. The passivity of the magnetic source makes it possible to have untethered tracking of the medical instrument. The localization system for passive magnetic tracking technology only requires arrays of magnetic sensors, which are widely used in the consumer products and consume much less power than the commercially available electromagnetic tracking system. Therefore, the localization system using passive magnetic tracking technology could be designed in a compact and wearable package with battery powered and wireless feature.

As aforementioned, the feasibility of the passive magnetic tracking in medical intervention has been experimentally validated. Comparing with those commercially available Electromagnetic tracking system (e.g. NDI Aurora), the developed passive magnetic tracking system has been proven capable of delivering comparable performance in terms of tracking accuracy and refresh rate, for example using the direct ANN method. However, the lacking of multiple objects tracking and 6-DOF tracking capabilities in the passive magnetic tracking technology is still criticized and considered as technical barriers in implementation. In the following, some of the recent development in these two areas in passive magnetic tracking are introduced.

5.1 Multiple Objects Tracking

One of the features of the commercial electromagnetic system is the capability of simultaneous tracking multiple sensors. Through a controlled varying electromagnetic field, voltages induced in the sensor coils can be differentiated and identified individually. For example, the NDI Aurora *V*3 System can be customized to provide simultaneous tracking of up to 16 sensors. On the opposite, in passive magnetic tracking, the system has less controlled variables to manipulate with since the magnetic sources are fixed. The identification of the multiple magnetic objects (sources) will depend on the algorithm only, as discussed in the following.

In general, when multiple magnetic objects coexist in free space, the principle of superposition applies. This concept simply means that the magnetic field in space is the sum of the contribution due to each magnetic source. Therefore, each magnetic object can be modeled as a single dipole as shown in Fig. 13. Although it is impossible to directly decouple the contributions from each magnetic source out of the total MFD measurements, the inverse optimization method can still be used by constructing a combined magnetic field model to calculate the most appropriate positions and orientations of each magnetic source. Based on Dipole Model, the total magnetic field at *i*th observation point due to *N* magnetic objects can be described as

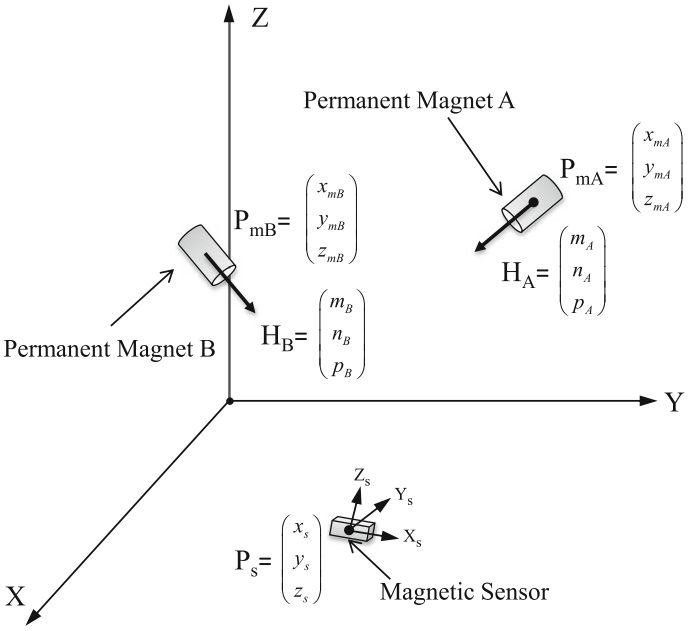

Fig. 13 Illustration of modeling each object as a single magnetic dipole.

$$\mathbf{B}(\mathbf{P}_{s_i}) = \sum_{j=1}^{N} \frac{\mu_r \mu_0 \cdot M_j}{4\pi} \left(\frac{3(\mathbf{H}_j \cdot \mathbf{P}_{ij})\mathbf{P}_{ij} - R_{ij}^3 \cdot \mathbf{H}_j}{R_{ij}^5} \right), \tag{12}$$

where μ_r is the relative permeability of the medium, μ_0 is the magnetic permeability of free space (mT· mm/A), M_j is the constant strength of the dipole moment (A· mm^2) for jth magnetic object, and $\mathbf{P}_{ij}$ is a vector from the jth magnetic object $\mathbf{P}_{m_j}$ pointing to the ith sensor $\mathbf{P}_s^i$, and R_{ij} is the magnitude of the vector $\mathbf{P}_{ij}$,

$$\mathbf{P}_{ij} = \mathbf{P}_{s_i} - \mathbf{P}_{m_j}. \tag{13}$$

A cost function C is then defined to quantify the differences between the measured and the modeled magnetic field at all k sensors in the sensor array:

By minimizing this cost function through iterative nonlinear optimization, the position vector $\mathbf{P}_m = [\mathbf{P}_{m_1}, \mathbf{P}_{m_2}, \ldots, \mathbf{P}_{m_N}]$ and orientation $\mathbf{H} = [\mathbf{H}_1, \mathbf{H}_2, \ldots, \mathbf{H}_N]$ of all N magnetic objects can be estimated from the sensor measurements.

Following the same definition as in (refeq:H), H_j represents a unit vector along the magnetized axis of the jth magnetic object, so the three components of H_j are actually correlated:

$$m_j^2 + n_j^2 + p_j^2 = 1. \tag{14}$$

Therefore, there are total of five independent variables in each dipole model (12), corresponding to the 5-DOFs tracking. Because of the axis-symmetric nature of the Dipole Model, only the Yaw and Pitch motions are represented. The Roll motion about the magnetized axis makes no differences in the magnetic field distribution.

Yang et al. first explored this method to simultaneously localize three identical magnets [24], such that the optimization problem could be simplified by sharing the same magnetic dipole strengths for all objects. But in such settings, it was difficult to distinguish the objects from each other, unless the initial positions of all objects were previously known. Recently, Song et al. used the same localization system to localize three magnets with different magnetic strength parameters [17]. The idea was verified in both simulations and experiments; but the magnets were assumed to be fixed in static.

At the current stage, only inverse optimization method could be applied due to the high uncertainties introduced by multiple objects. And the number of magnets also needs to be pre-defined and fixed; otherwise the likelihood of the optimization cost function converging to local minimum increases with the increasing number of unknown parameters. Due to such complexity, the processing time would also be affected. Along this research direction, it is expected to have a fast and robust algorithm to identify the number of objects as well as to estimate their positional information (both position and orientation) with reasonable accuracy.

5.2 6-DOF Tracking

As stated previously, 5-DOF tracking in magnetic tracking is the most common one since the magnetic field is usually symmetric about the magnetization axis of the magnet. In order to have 6-DOF tracking to include the roll motion, the commercial electromagnetic tracking system incorporates two sensor coils perpendicularly to each other; thus, by tracking the positional information of both sensor coils simultaneously, all 6-DOF parameters could be recovered.

Similar concept could be used in passive magnetic tracking to enable 6-DOF tracking. Song et al. reported using assembly of two identical perpendicular aligned permanent magnets inside a wireless capsule endoscopy (WCE) [19]. Dipole model was used and two magnets were localized separately with constraints on the parameters. However, due to the limitation of the dipole model, there would be no unique solutions if two magnets are too close to each other; the estimated orientation errors would be large. Thus, the two perpendicular aligned magnets have to be kept at a distance. For example, in [19], the two magnets were placed 10cm apart from each other.

Another method to enable 6-DOF tracking in passive magnetic tracking is to adopt a better physical model that is able to take account of the geometry rather than dipole model. Then an odd geometric shaped magnet can be used to bring asymmetry in the magnetic field about the magnetization axis. For example, Yang et al. suggested using a thin rectangular shape magnet [25] and Song et al. suggested using a diametrically magnetized long annular shape magnet [18]. But only simulation results were presented as concept verification. But in their work, the simulation also shown that the differences in the magnetic field asymmetry caused by the geometry of the magnet could be quite limited; compared to the dipole model, the differences at a distance away from the magnet could be only in $10^{-}2\mu$T level which could be hardly picked up by the magnetic sensors.

Following the idea used in the active electromagnetic tracking, one novel idea to amplify such asymmetry in the magnetic field is to use magnet assembly. As shown in Fig. 14, three different assembly designs are presented to form two mutually orthogonal magnetic fields by using axially and diametrically magnetized magnets.

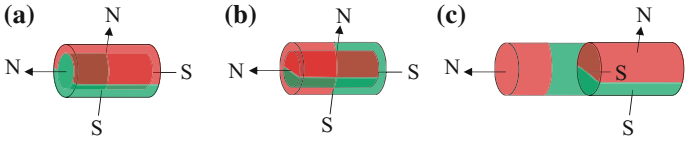

Fig. 14 Three different magnet assembly designs **a** Axially magnetized cylindrical magnet inside diametrically magnetized annular magnet **b** Diametrically magnetized cylindrical magnet inside axially magnetized annular magnet **c** Two cylindrical magnets with axially and diametrically magnetized each.

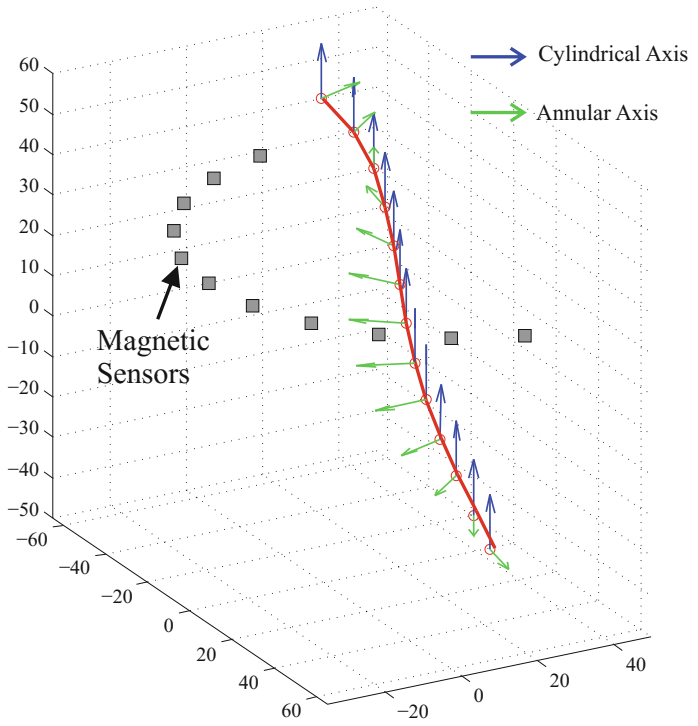

Fig. 15 Performance of 6-DOFs tracking using Charge Model.

- An axially magnetized cylindrical magnet inside a diametrically magnetized annular magnet.
- A diametrically magnetized cylindrical magnet inside an axially magnetized annular magnet.
- An axially magnetized magnet in serial with a diametrically magnetized magnet.

Then the charge model could be used to represent the actual magnetic field of the assembly. The derivation of the magnetic field of a cylindrical/annular magnet using the charge model can be found in the Appendix. Taking the assembly design A as an example, a simulation is performed as follows. Based on the specifications from magnet manufacturer K& J Magnetics, one axially magnetized cylindrical magnet (D28-N52), and one diametrically magnetized annular magnet (R424-DIA) are chosen. The radius of the cylindrical magnet is the same as the inner diameter of the annular magnet. Using the nasogastric intubation application as reference, the simulation is performed with the cylindrical magnet pointing upward straight with magnetization at [0, 0, 1], while the annular magnet rotating around the Z-axis. The results are shown in Figs. 15 and 16.

As shown in Fig. 15, the proposed method is able to detect three positions as well as the three orientation of the assembly. Figure 16 shows the position and orientation

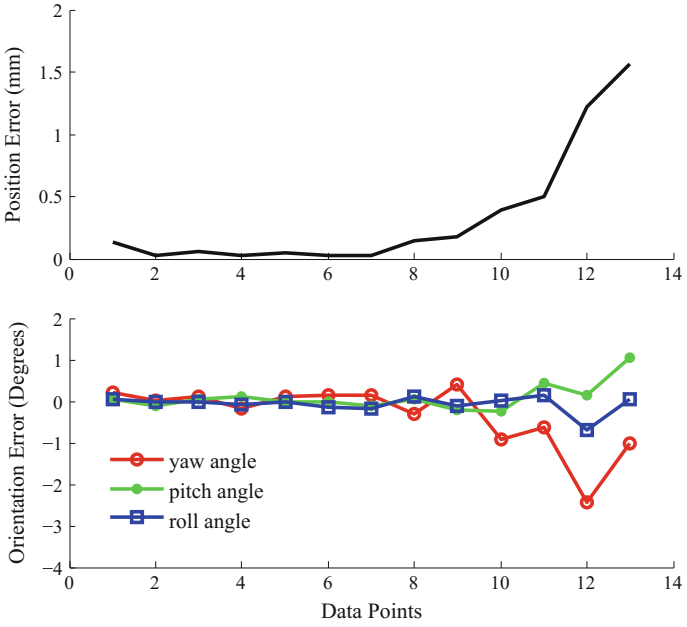

Fig. 16 Tracking errors of 6-DOFs tracking using Charge Model (top) position error (bottom) orientation error.

errors at each data point. It is noted that the error becomes larger as the assembly moves further away from the sensor array. That is expected as the further away from the sensor array, the larger the Signal-to-Noise Ratio (SNR); thus, the tracking accuracy will be affected.

The concept of 6-DOF tracking in passive magnetic tracking has been theoretically verified. The next step is to validate this method using experimental data. One foreseen limitation would be the processing time due to the iterative calculation using the complex physical models. For example, adoption of the charge model would result in hectic computation load of the integration in the optimization stage. A computationally inexpensive model would be desired to solve this problem.

6 Conclusion

In this chapter, the concept of passive magnetic tracking technology has been presented. The advantages of using permanent magnets as passive magnetic source for medical intervention localization are explored. Comparing with the commercially available active electromagnetic tracking systems, it is shown that the passive magnetic tracking technology is able to provide comparable performance in terms of the tracking accuracy and refresh rate. The challenges and limitations in the current

development of this technology were also discussed. It is expected that the passive magnetic tracking technology could open a new era in the design and development for instrument localization in medical interventions, This would allow for less modification and invasiveness in the current routine, enable untethered / mobile system design and target better ergonomics and cost-efficiency.

Acknowledgements The work is supported by SUTD-MIT International Design Center (IDC) Research Grant IDSF1200107OH, and partially support by the State Joint Engineering Lab on Robotics and Intelligent Manufacturing (2015[581], 2015[955]), and Shenzhen Engineering Lab on Robotics and Intelligent Manufacturing (2014[1722]).

Appendix

Magnetic Field of a Cylindrical Magnet Using the Charge Model

In order to calculate the surface integration of a cylindrical magnet, the variables are first transformed into cylindrical coordinates by

$$\begin{aligned} x_c &= r \cdot cos(\theta) \\ y_c &= r \cdot sin(\theta) \\ z_c &= z. \end{aligned} \tag{15}$$

For a cylindrical axially magnetized magnet, only the top and bottom surfaces are considered since the outward surface vector of the lateral surface is perpendicular to the magnetized vector, thus $\mathbf{M} \cdot \hat{\mathbf{n}} = 0$. Let the magnetization be $\mathbf{M} = M_s\hat{\mathbf{z}}$, then it can be obtained $\sigma = M_s$ for the top surface ($z_{c_{top}} = h/2$), $\sigma = -M_s$ for the bottom surface ($z_{c_{bottom}} = -h/2$). The magnetic field at observation point $\mathbf{P}_s$ can be written as

$$\begin{aligned} \mathbf{B}(\mathbf{P}_s) = &\frac{\mu_0 M_s}{4\pi} \int_0^{2\pi} \int_0^R \frac{\mathbf{P}_s - \mathbf{P}_{c_{top}}}{|\mathbf{P}_s - \mathbf{P}_{c_{top}}|^3} \, r dr d\theta \\ &- \frac{\mu_0 M_s}{4\pi} \int_0^{2\pi} \int_0^R \frac{\mathbf{P}_s - \mathbf{P}_{c_{Bottom}}}{|\mathbf{P}_s - \mathbf{P}_{c_{Bottom}}|^3} \, r dr d\theta. \end{aligned} \tag{16}$$

For a cylindrical diametrically magnetized magnet, only the lateral surface is considered. Let the magnetization be $\mathbf{M} = M_s\hat{\mathbf{y}}$. The outward normal vector at the lateral surface can be written as

$$\hat{\mathbf{n}} = cos(\theta)\hat{\mathbf{x}} + sin(\theta)\hat{\mathbf{y}}. \tag{17}$$

Then the surface charge density equals to

$$\begin{aligned}\sigma &= \mathbf{M} \cdot \hat{\mathbf{n}} \\ &= M_s \hat{\mathbf{y}} \cdot (cos(\theta)\hat{\mathbf{x}} + sin(\theta)\hat{\mathbf{y}}) \\ &= M_s\, sin(\theta).\end{aligned} \tag{18}$$

The magnetic field at point $\mathbf{P}_s$ can be calculated

$$\mathbf{B}(\mathbf{P}_s) = \frac{\mu_0 M_s}{4\pi} \int_0^{2\pi} \int_{-h/2}^{h/2} \frac{\mathbf{P}_s - \mathbf{P}_c}{|\mathbf{P}_s - \mathbf{P}_c|^3} \, R dz d\theta \tag{19}$$

For an annular magnet, its magnetic field can be obtained by the principle of superposition. It is equivalent to the magnetic field of a cylindrical magnet with the size of the outer diameter subtract that of a cylindrical magnet with the size of the inner diameter.

References

1. Baldoni, J.A., and B.B. Yellen. 2007. Magnetic tracking system: Monitoring heart valve prostheses. *IEEE Transactions on Magnetics* 43 (6): 2430–2432.
2. Bercik, P., et al. 2005. Noninvasive verification of nasogastric tube placement using a magnet-tracking system: A pilot study in healthy subjects. *Journal of Parenteral and Enteral Nutrition* 29 (4): 305–310.
3. Bishop, C.M. 1996. *Neural networks for pattern recognition*, 1st ed. Oxford University Press.
4. Franz, A.F., et al. 2014. Electromagnetic tracking in medicine-a review of technology, validation and applications. *IEEE Transactions on Medical Imaging* 33 (8): 1702–1725.
5. Furlani, Edward P. 2009. *Permanent magnet and electromechanical devices: Materials, analysis and applications*, 1st ed. Academic Press.
6. Hu, C., T. Ma, and M.Q.-H. Meng. 2007. Sensor arrangement optimization of magnetic localization and orientation system. In *IEEE International Conference on Integration Technology*, pp. 311–315.
7. Hu, Chao, M.Q.-H. Meng, and Mrinal Mandal. 2005. Efficient magnetic localization and orientation technique for capsule endoscopy. *International Journal of Information Acquisition* 2 (1): 23–36.
8. Lee, K.-M., and Min Li. 2013. Magnetic field localization method for guiding visually impaired applications. In *IEEE/ASME International Conference on Advanced Intelligent Mechatronics*, pp. 542–547.
9. Lee, K.-M., Min Li, and Chun-Yong Lin. 2015. A novel way-finding method based on geomagnetic field effects and magnetic tensor measurements for visually impaired users. In *IEEE/ASME International Conference on Advanced Intelligent Mechatronics*, pp. 232–237.
10. Lee, K.-M., and H. Son. 2007. Distributed multipole model for design of permanentmagnet-based actuators. *IEEE Transaction on Magnetics* 43 (10): 3904–3913.
11. Maréchal, L., et al. 2016. Design optimization of a magnetic field-based localization device for enhanced ventriculostomy. *Journal of Medical Devices* 10 (1).
12. Maréchal, L., et al. 2015. Design optimization of the sensor spatial arrangement in a direct magnetic field-based localization system for medical applications. In *IEEE International Conference on Engineering in Medicine and Biology Society*, pp. 897–900.

13. Maréchal, L., et al. 2014. Optimal spatial design of non-invasive magnetic field-based localization systems. In *IEEE International Conference on Robotics and Automation*, pp. 3510–3516.
14. Meng, M.Q.-H., et al. 2004. Wireless robotic capsule endoscopy: state-of-the-artand challenges. In *World Congress on Intelligent Control and Automation*, pp. 5561–5565.
15. Schlageter, V., et al. 2001. Tracking system with five degrees of freedom using a 2D-array of Hall sensors and a permanent magnet. *Sensors and Actuators A: Physical* 92 (1–3): 37–42.
16. Sharma, A.B., L. Golubchik, and R. Govindan. 2010. Sensor faults: Detection methods and prevalence in real-world datasets. *ACM Transactions on Sensor Networks* 6 (3).
17. Song, S., C. Hu, and M.Q.-H. Meng. Multiple objects positioning and identification method based on magnetic localization system. *IEEE Transactions on Magnetics*. https://doi.org/10.1109/TMAG.2016.2583408.
18. Song, S., et al. 2014. 6-D magnetic localization and orientation method for an annular magnet based on a closed-form analytical model. *IEEE Transactions on Magnetics* 50 (9): 1–11.
19. Song, S., et al. 2009. Two-Magnet-based 6D localization and orientation for wireless capsule endoscope. In *IEEE International Conference on Robotics and Biomimetics*, pp. 2338–2343.
20. Sun, Z., et al. 2015. A non-invasive real-time localization system for enhanced efficacy in nasogastric intubation. *Annals of Biomedical Engineering* 43 (12): 2941–2952.
21. Sun, Z., et al. 2016. Real-time sensor fault detection and compensation in a passive magnetic field-based localization system. In *IEEE/ASME International Conference on Advanced Intelligent Mechatronics*, pp. 1040–1046.
22. Wang, X., M.Q.-H. Meng, and Y. Chan. 2006. A localization method using 3-axis magnetoresistive sensors for tracking of capsule endoscope. In *IEEE International Conference on Engineering in Medicine and Biology Society*, pp. 2522–2525.
23. Wu, F., S.H. Foong, and Z. Sun. 2015. A hybrid field model for enhanced magnetic localization and position control. *IEEE Transactions on Mechatronics* 20 (3): 1278–1287.
24. Yang, W., et al. 2010. A new tracking system for three magnetic objectives. *IEEE Transactions on Magnetics* 46 (12): 4023–4029.
25. Yang, W., et al. 2009. A six-dimensional magnetic localization algorithm for a rectangular magnet objective based on a particle swarm optimizer. *IEEE Transactions on Magnetics* 45 (8): 3092–3099.
26. Yao, W.-S., et al. 2012. Detection of magnetic object movements by flux density tracking control. *IEEE/ASME Transactions on Mechatronics* 17 (4): 709–716.